6724 *Macromolecules* **2010**, *43*, 6724–6730
DOI: 10.1021/ma1011254

Macromolecules
ARTICLE

Morphology Mapping of Phase-Separated Polymer Films Using Nanothermal Analysis

M. P. Nikiforov,*,† S. Gam,‡ S. Jesse,† R. J. Composto,‡ and S. V. Kalinin†

†*The Center for Nanophase Materials Sciences, Oak Ridge National Laboratory, Oak Ridge, Tennessee 37831, and* ‡*Department of Materials Science and Engineering, University of Pennsylvania, Philadelphia, Pennsylvania 19104*

Received May 20, 2010; Revised Manuscript Received July 9, 2010

ABSTRACT: Polymers films are attractive, in part, because their physical properties can be tuned by blending polymer with complementary characteristics. However, blending is typically challenging because most polymers will undergo phase separation, resulting in unpredictable behavior. Here, we introduce band excitation nanothermal analysis (BE-NanoTA) as a nondestructive AFM-based technique for mapping the near surface, thermal properties of polymeric coatings. BE-NanoTA was used to investigate phase separation and domain growth in poly(styrene-*ran*-acrylonitrile):poly(methyl methacrylate) SAN: PMMA films. The size and shape of PMMA-rich domains are consistent with prior measurements on the same system using a destructive method, namely UV-ozone etching of PMMA followed by topography mapping using standard AFM. Moreover, new insights into the mechanism of phase separation were uncovered including the observation of SAN- and PMMA-rich channels near the surface at early times as well as small SAN-rich domains trapped within large PMMA domains during intermediate times. Because it is nondestructive, BE-NanoTA can be used to explore in situ phase evolution in soft matter systems (e.g., polymer nanocomposites) which do not lend themselves to the UV-ozone etching method.

Introduction

Polymer thin films are utilized in many present-day technologies[1,2] because they exhibit attractive physicochemical properties. By combing mixtures of polymers, new combinations of properties can be achieved that impart the materials with functionality, improved processability, and lower cost. However, the targeted properties of polymer mixtures can be perturbed because of phase separation, phase coarsening, and interfacial segregation under exposure to environmental conditions such as heat, moisture, and pressure.[3] Monitoring the spatial distribution of the glass transition temperatures across a sample can be used to identify the coexisting phases. Conventional methods for determining the glass transition temperature in phase separated systems require large samples, ~milligrams, and large domains.[4,5] Moreover, these methods are typically not appropriate for thin films, particularly those having phases with sizes on the order of tens of nanometers. Although several methods with submicrometer spatial resolution are available, such as transition temperature microscopy (TTM)[6,7] and NEXAFS microscopy,[8] these methods are either lacking resolution for characterization of submicrometer domain size in multiphase systems (e.g., TTM) or requiring expensive equipment (e.g., NEXAFS). Recent experiments suggest that nanoconfinement of the polymer near interfaces, such as vacuum−polymer and substrate−polymer, results in a change of structural relaxation and the local glass transition temperature.[9] The glass transition in polymers is associated with a large change in mechanical properties.[10,11] Atomic force microscopy (AFM) is an attractive platform for investigating the glass transition in polymer films by mapping the mechanical properties with high resolution and spatial distribution at sub-100 nm resolution, a routine exercise for AFM.[12] Although attempts have been made,[13] the mechanical properties of polymers as a function of temperature have not been mapped at high resolution. Local measurements of the mechanical properties of polymers as a function of temperature have only been recently demonstrated.[14,15] Here, we show that AFM-based band excitation nanothermal analysis (BE-NanoTA) can be used to measure the mechanical properties and glass transition temperature in the near surface region with a point-to-point lateral resolution of 50 nm. Specifically, BE-NanoTA analysis confirms the results from prior experiments showing that poly(styrene-*ran*-acrylonitrile) (SAN):poly(methyl methacrylate) (PMMA) films undergo an early and intermediate stage of phase separation. Moreover, BE-NanoTA provided new observations including SAN- and PMMA-rich channels near the surface at early times as well as SAN-rich domains trapped within PMMA domains that span the film during intermediate times.

Experimental Section

Implementation of BE-NanoTA. BE-NanoTA technique consists of four main components: a Veeco Multimode™ atomic force microscope (AFM) equipped with a Nanonis controller; an in-house developed MatLab/LabView data acquisition and control system; tip heating protocol and nanoheater placed on the AFM tip. Anasys Instruments heated probes (AN2−300) were used for the experiments (cantilever spring constant ~0.5 N/m). Heating of the probe was done using the MatLab/LabView control system. The heating protocol is a sum of two heating signals: dc heating and ac heating. The ac heating excitation band spanning approximately 100−500 kHz (increasing chirp)[37] with an amplitude 0.2−0.5 V was used to generate temperature modulations of the tip. Constant 10 °C temperature amplitude of ac heating was maintained by changing

*To whom correspondence should be addressed.

 Published on Web 07/22/2010

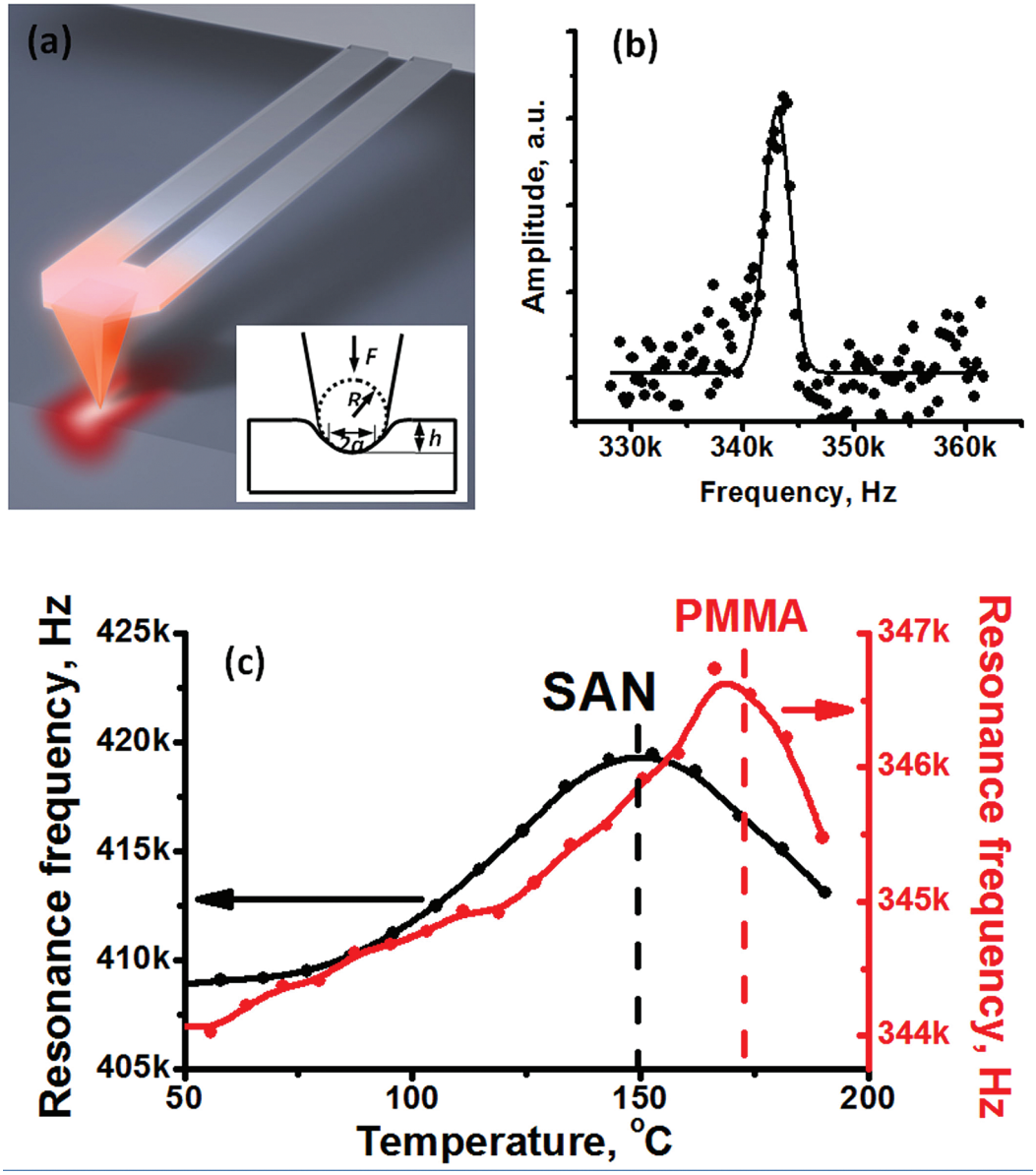

Figure 1. Cantilever schematic and analysis used in BE-NanoTA. (a) A heated tip locally heats the near surface of the film. The inset shows the contact mechanics model used for contact resonance frequency, contact area, and Young's modulus. (b) Amplitude of tip oscillations in vertical plane as a function of frequency caused by thermal expansion of the material under the tip. Simple harmonic oscillator (SHO) model fits contact resonance behavior well (black line is SHO fit). SHO model was used for determination of contact resonance frequency. (c) Contact resonance frequency as a function of temperature for pure PMMA and SAN films. Regions A, B, and C denote glassy state, glass transition region, and melt state The resonance frequency decreases as the polymer softens signifying that the near surface glass transition has been observed.

amplitude of ac heating voltage. A tip experiences periodic (ac) heating, while in contact with the surface, resulting in the periodic thermal expansion of the underlying material (Figure 1a,b). The usual length of the ac heating wave is ~1 s. The linear expansion coefficients (α) for SAN and PMMA are $(2-6) \times 10^{-4}$ K^{-1} [33] and $(1-2) \times 10^{-4}$ K^{-1},[34,35] respectively. Thermal expansion of the polymer under the tip causes displacement of the tip normal to the surface plane. Assuming the ac heat wave propagates ~20 nm below the surface and $\Delta T \sim 10$ °C, the amplitude of induced tip oscillations is on the order of 100 pm (within detection range of AFM photodetector). Thermal expansion of the material is measured using vertical displacement signal from Veeco Multimode™ AFM, when tip is heated and pushed on the surface with a force of hundreds of nanonewtons. The heating waveform contains band of frequencies centered at the contact resonance of tip−sample system (100−500 kHz). The mechanical response of the system is recorded by measuring and digitally storing the motion of the tip, taking the Fourier transform of the response. The amplitude, resonance frequency, and quality factor were extracted using a simple harmonic oscillator model at regular intervals during the tip heating process. The resonance frequency of the tip oscillations is proportional to the stiffness of the tip−surface contact. We probed resonance behavior of the mechanical response of the tip−surface junction by changing the temperature of the tip with 10 °C amplitude in oscillatory fashion (for more details see ref 25). This approach allows us to probe the tip resonance−surface contact as a function of temperature (Figure 1c). The mechanical response of the tip while in contact with the surface was probed by applying dc heating with a temperature step of ~4 °C, simultaneously with the periodic ac heating.

Temperature Calibration of the Heated Probe. Because of the difference thermal impedance between the cantilever and tip, the temperature of the tip may be different from the temperature of the cantilever. In this work we use the standard polymeric samples (polycarbolactone (PCL), high-density polyethylene

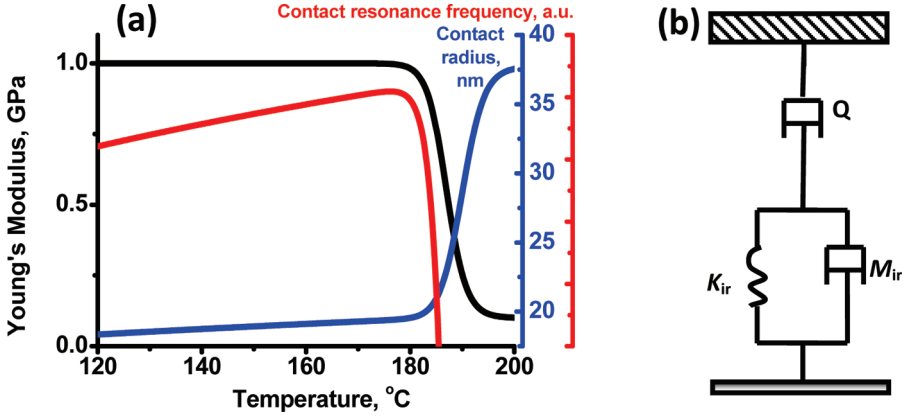

Figure 2. (a) Dependence of contact resonance frequency on temperature and Young's modulus was modeled according to the Hertzian + creep model described in the text. Initial slow increase in the contact radius is due to creep of polymer (after ref 24); sharp increase at temperature higher than 180 °C is due to decrease in Young's modulus (Hertzian model). (b) Mechanical model used for description of polymer creep.

(HDPE), and poly(ethylene terephthalate) (PET)) with known melting temperatures to calibrate the temperature at the tip under static excitation.[25] This approach for calibrating the dynamic transfer function was pioneered by Lee et al.[38]

Mathematical Analysis of the Data. Glass transition temperature maps were created from temperature dependencies of resonance frequency. Global maximum on the resonance frequency curve was found after interpolation of the temperature dependence of resonance frequency by the fourth-order polynomial using MatLab routine.

Sample Preparation. Individual polymers poly(methyl methacrylate) (PMMA) and poly(styrene-*ran*-acrylonitrile) (SAN) having an AN content of 33 wt % were obtained from Polymer Source and Monsanto. PMMA was used as received and SAN was purified before use. During purification SAN transparent pellets were dissolved in chloroform, and the SAN−chloroform solution was added drop by drop into methanol for precipitation. The SAN precipitate was dried at room temperature under the vacuum for 24 h. The weight-average molecular weights and polydispersities of PMMA and SAN are 82.4 kg/mol and 1.07 and 118 kg/mol and 2.24, respectively. A blend of PMMA and SAN with 1:1 weight ratio was investigated. The mixture of PMMA and SAN powder (1:1 weight ratio) was dissolved in methyl isobutyl ketone (MIBK), spin-cast on a silicon wafer, and dried at 120 °C in a vacuum for 24 h to evaporate the MIBK. The thickness of spin-cast films was measured using an ellipsometer. The films were annealed on a hot stage (Mettler FP-82, Mettler Toledo) at 195 °C in an argon atmosphere and quenched to room temperature, far below the glass transition temperature of PMMA and SAN. The PMMA:SAN blend used has a lower critical solution temperature of ~160 °C and upon annealing at 195 °C separates into nearly pure PMMA and SAN phases.[30] Quenching below T_g is rapid relative to remixing kinetics, and therefore the morphology observed at room temperature is representative of the phase-separated structure. Surface morphologies of these films were measured using tapping mode AFM.

DSC Analysis. DSC analysis of pure polymer components was performed using TA Instruments Q2000 in a He atmosphere. Approximately 3 mg of pure polymer component (SAN or PMMA) was placed in an aluminum pan. The scanning temperature range was 30−200 °C with a temperature ramp of 10 °C/min.

Results and Discussion

Previous studies showed that SAN:PMMA blend undergoes early, intermediate, and late stages of phase evolution (see Supporting Information for details).[16−19] BE-NanoTA was applied to study SAN:PMMA phase separation by mapping the temperature dependence of mechanical properties and determine the glass transition temperature in the near surface region of the coating. BE-NanoTA is an extension of scanning thermal expansion microscopy (SThEM), where periodic heating of the tip surface junction results in periodic local thermal expansion of the substrate.[20] BE-NanoTA periodically heats the tip and determines the mechanical properties of the material (Young's modulus and viscoelasticity) as a function of temperature by measuring changes in the resonance frequency, amplitude, and quality factor of the AFM cantilever in contact with the surface. As shown in Figure 1, BE-NanoTA uses an AFM probe with a heater that contacts the surface (Figure 1a). The contact resonance parameters, such as frequency, are measured locally (i.e., at the tip−surface interface; Figure 1b presents typical frequency response of tip oscillation amplitude to temperature excitation) as a function of temperature (Figure 1c). Next, the glass transition temperature is determined as a maximum on temperature dependence of resonance frequency.

On the basis of the theory of contact mechanics,[22] the contact stiffness changes if the contact area and/or Young's modulus change during heating. The glass transition due to local relaxations of the polymer chain correlates with a change from a solid-to-melt state upon heating and a corresponding decrease of Young's modulus by ~3 orders of magnitude over a fairly narrow temperature range.[10,11,23] Thus, the decrease of Young's modulus (i.e., decrease in the resonance frequency) can be used to determine the glass transition temperature of the polymer or phase adjacent to the tip. The initial increase in resonance frequency (Figure 1c) results from an increase in tip−surface contact area associated with the thermal expansion of the glassy polymer. As shown in Figure 1c, a sharp decrease in resonance frequency occurs when the surface region under the tip undergoes a solid to melt transition. Figure 2 shows the relationship between the resonant frequency and modulus.

Theoretical modeling of the contact mechanics at the tip−surface junction is required to understand how the contact resonance frequency depends on temperature. Initially as the tip approaches the surface, the contact radius ($R_{contact}$) is determined by the Hertzian model (eq 1):[22]

$$R_{contact} = \left(\frac{3FR_{tip}}{4E(T)}\right)^{1/3} \quad (1)$$

where R_{tip} is the tip radius (50 nm), F is the indentation force (1000 nN), and $E(T)$ is Young's modulus (~1 GPa for PMMA at 20 °C). During heating, the force between the tip and surface is constant and the polymer creeps. Previous studies[24]

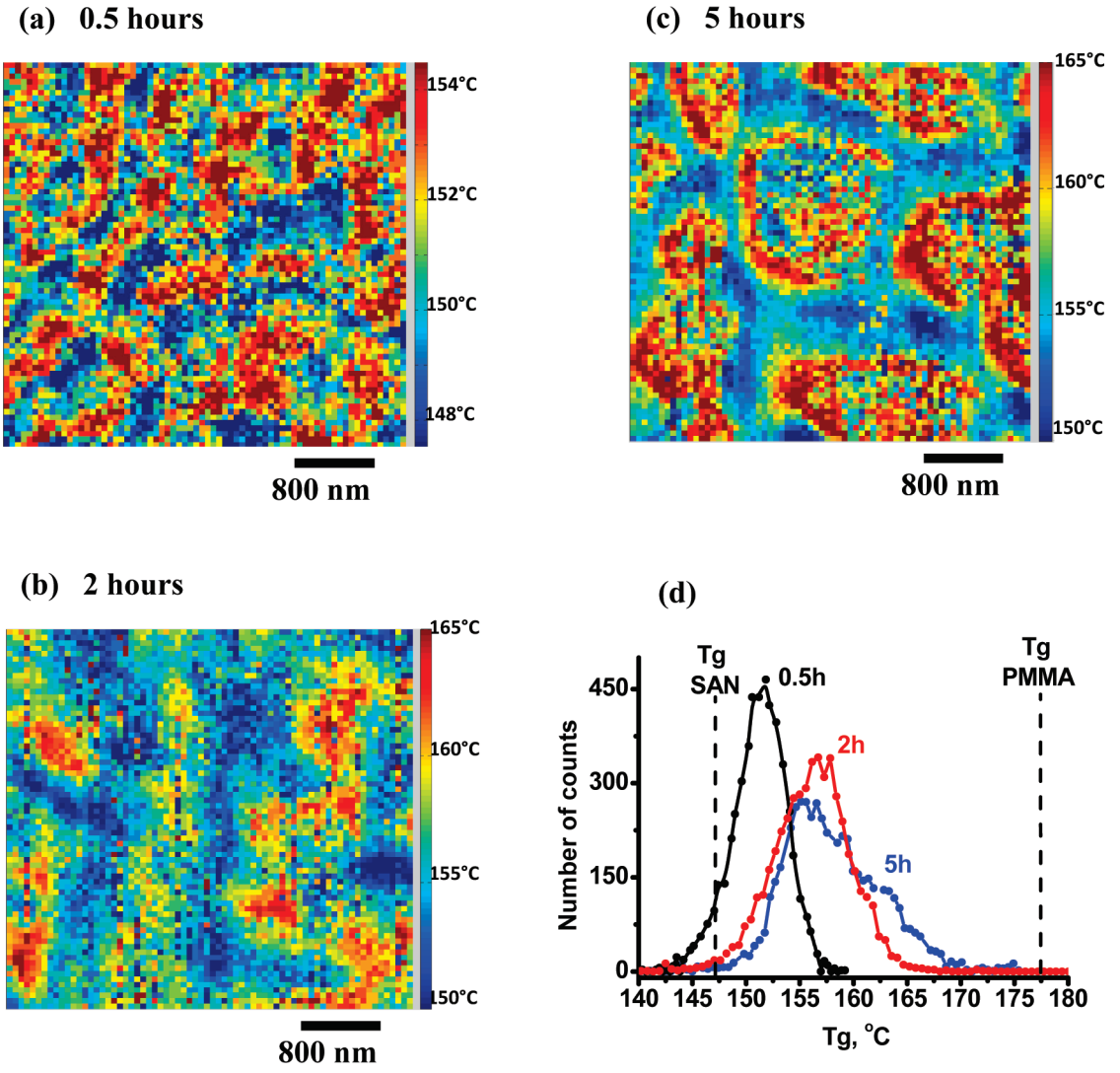

Figure 3. Maps of the glass transition temperature across the surface of PMMA:SAN films during the early and intermediate stages of phase separation represented by (a) 0.5, (b) 2, and (c) 5 h. The PMMA-rich and SAN-rich domains are denoted as red and blue corresponding to high and low glass transition temperature regions. Initially, the PMMA domains are elongated (early stage) and evolve into circular domains at 2 and 5 h (intermediate state). The scan size is 4.1 μm × 3.8 μm. (d) Histograms of the glass transition temperatures extracted from the spatially resolved maps in (a−c).The dashed lines represent the glass transition temperatures measured for pure SAN and pure PMMA films. After 5 h, the phases have sufficiently evolved so that two separate glass transition temperatures appear. The wetting layer of PMMA (100 nm and less) confounds an exact mapping of the measured T_g with the corresponding phase. The shape of glass transition temperature distribution histograms is similar for samples annealed at 0.5 and 2 h, when the difference in domain structure of these samples is substantial (a, b). This illustrates the importance of high-resolution T_g mapping and added benefits of BE-NanoTA comparing with bulk methods of thermal analysis for studies of polymer phase separation.

quantified the creep in PMMA using an irreversible deformation model:

$$h^2 = \frac{F}{K_{ir}} + \frac{FM_{ir}}{t_1 K_{ir}^2}\left(\exp\left(-\frac{tK_{ir}}{M_{ir}}\right) - \exp\left(-\frac{(t-t_1)K_{ir}}{M_{ir}}\right)\right) + \frac{F}{2Qt_1}t^2 - \frac{F}{2Qt_1}(t-t_1)^2 \quad (2)$$

where h is indentation depth, t_1 is time when force stops increasing (1s), K_{ir} is the stiffness in the Kelvin model (18.3 GPa), M_{ir} is the dashpot parameter (109 GPa/s), and Q is the dashpot parameter (711 GPa/s).[24] Creep (h) was calculated using the Kelvin model in series with the dashpot (Figure 2b). From $h(t)$, the change in contact radius ($R_{contact}$) as a function of time can be calculated assuming a spherical tip with radius, R = 50 nm (Figure 2). For simplicity, we assumed that contact radius is the sum of Hertzian contact radius (eq 1) and contact radius due to creep. The change in the Young's modulus of polymer was modeled using the sigmoidal shaped function with transition temperature ~180 °C, and the change in Young's modulus from 1 GPa to 100 MPa to illustrates the change in contact resonance frequency as a function of Young's modulus and temperature. Resonance frequency (f_{res}) was calculated following refs 14 and 25:

$$f_{res} = \left(1 - 7.7\frac{k_{tip}}{k_{cont}}\right) f_{bound} \quad (3)$$

where k_{tip} is the spring constant of the tip (1 N/m) and k_{cont} the contact stiffness, $k_{cont} = 2R_{contact}E$. The modeling (Figure 2) is consistent with the behavior of the resonance frequency as a function of temperature. Initially, the resonance frequency increases due to the thermal expansion of the glassy polymer that increases the tip−surface contact area. As the polymer undergoes a glass to rubber transition, the contact resonance frequency decreases sharply (50−200 Hz/K) as the modulus decreases in the region around the tip−surface contact area.

Before testing heterogeneous films, BE-NanoTA was used to determine the glass transition temperature of homogeneous SAN and PMMA films. The T_g values are 147 and 177 °C,

Table 1. Glass Transition Temperatures of PMMA and SAN Measured Using DSC and BE-NanoTA[a]

	T_g(0.17 Hz), °C (DSC)	T_g(300 kHz), °C (BE-NanoTA)	ΔT_g, °C	T_r, °C	activation enthalpy, kJ/mol
PMMA	131	177	46	154	469
SAN	114	147	33	131	582

[a] Activation enthalpy of the glass transition calculated from ΔT_g.

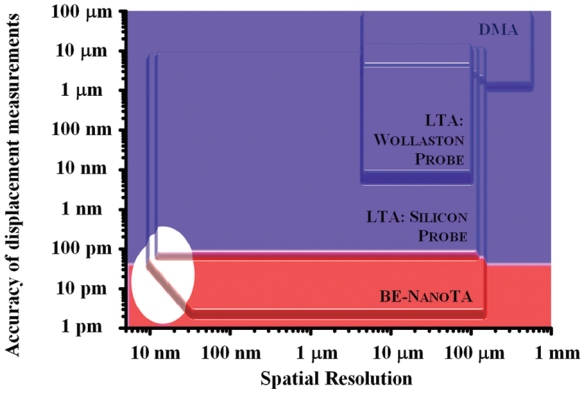

Figure 4. Comparison of thermomechanical analysis methods and potential applications. The sensitivity in displacement measurements and spatial resolution for DMA, LTA: Wollaston probe, LTA: silicon probe, and BE-NanoTA. The accuracy in displacement measurements and spatial resolution required for different applications, including the mechanical properties of the surfaces, analysis of pharmaceuticals, lithography masks, organic layers in OLEDs (blue/dark gray rectangle). Fundamental studies include the mechanics of single molecules (white/light ellipse); ferroelectric transitions and thermal expansion of the materials (red/light gray rectangle).

respectively, and provide the minimum and maximum values expected for the heterogeneous system. These limits are noted as dashed lines in Figure 3d. For a heating rate of 10 °C/min, the DSC values of bulk SAN and PMMA are 114 and 131 °C, respectively. Because BE-NanoTA uses a much higher heating rate ~100 000 °C/s, the T_g values are much greater than those from DSC. Using the standard deviation of several measurements over a 10 μm × 10 μm area, the T_g values determined by BE-NanoTA are reproducible to within 3 °C. Moynihan et al. showed that the glass transition temperature T_g is related to the heating or cooling rate $|q|$ by

$$\mathrm{d}\ \ln|q|/\mathrm{d}T_g = \Delta h/RT_r^2 \qquad (4)$$

where T_r is a temperature in the middle of the transition range and Δh is the activation enthalpy for the relaxation times controlling the structural enthalpy or volume relaxation.[26] Activation enthalpies for glass transition process were calculated for PMMA and SAN materials using eq 4 and the experimental glass transition temperatures (Table 1). The activation enthalpy for PMMA is 469 kJ/mol, in agreement with literature values which range from ~350 to 800 kJ/mol.[27−29] This agreement suggests that the transition temperatures from the BE-NanoTA method are consistent with the glass transition temperatures of the respective polymers at high frequency. No literature values for SAN were found.

The spatial distribution of glass transition temperatures was measured across the surface of a phase-separated poly(methyl methacrylate) (PMMA):poly(styrene-*ran*-acrylonitrile) (SAN) blend film with a thickness of 350 nm. The surface morphology of PMMA:SAN was determined by BE-NanoTA as well as by conventional (topography and phase) AFM. Films were annealed at 195 °C and quenched to room temperature, far below the glass transition temperature of PMMA and SAN (see Experimental Section for more details). At 195 °C, this blend separates into coexisting phases of nearly pure PMMA and SAN because this temperature is about 35 °C above the lower critical solution temperature of PMMA:SAN mixture.[30] For the as-cast (0 h) film, the glass transition map showed almost no spatial variation of T_g (image not shown) and an average value of 150 °C ± 3 °C (3 μm × 3 μm). This observation is consistent with a homogeneous surface, where the softening temperature of the material is determined by the lowest softening temperature of the components. After annealing for 0.5 h the PMMA:SAN blend undergoes phase separation with the formation of irregularly shaped PMMA domains (red) with widths ranging from 500 to 1000 nm (Figure 3a). As shown in Figure S1b (Supporting Information) and described in previous studies,[16−19,31] the topographical variation reflects the domains near the outermost ~200 nm of the surface. Qualitatively, the glass transition temperature map in Figure 3a correlates with the topography and phase maps. Namely, the high and low regions in the topography image (Figure S1b, Supporting Information) correspond to the PMMA-rich (high T_g) and the SAN-rich (low T_g) regions in Figure 3b. As expected, with further annealing (Figure 3b,c), the domain size of PMMA increases from ~600 to ~1500 nm. Thus, the BE-NanoTA measurements support the proposed mechanism for phase separation during the intermediate stage characterized by growth of PMMA domains.

Upon comparing films annealed for 0.5 and 2 h, a map of the glass transition temperature across the surface of the phase-separated films shows that the T_g contrast increases as the phase size increases and becomes more discrete. To understand this behavior, the T_g variations across all three samples are presented in Figure 3d. Whereas the T_g distribution for 0 (not shown), 0.5, and 2 h are monomodal with average temperatures 150, 152, and 157 °C, respectively, the distribution after 5 h is bimodal with average temperatures of 155 and 165 °C. The observation of a biphasic T_g at longer times indicates that the phase size is large enough to be easily distinguished when plotted in this manner. According to the phase separation model for PMMA:SAN, the SAN domains in the midlayer are covered with wetting layer of PMMA, which reaches a maximum thickness of about 100 nm at the end of the early stage and steadily thins during the intermediate stage as PMMA flows from the wetting layer into the PMMA domains below.[18] Because our technique is sensitive to the outer surface region (~200 nm), this wetting layer limits our ability to correlate the T_g's from the blend with those of the pure components. Nevertheless, Figure 3a−c clearly shows PMMA-rich (high T_g/red) and SAN-rich (low T_g/blue) regions and that these regions become larger and more circular with annealing.

Two new details of phase separation in PMMA:SAN films were uncovered by BE-NanoTA. After 2 and 5 h of annealing, the SAN phase (blue) is continuous whereas after 0.5 h the SAN phase is highly elongated and possibly discrete. This latter observation may reflect that the bicontinuous structure characteristic of the early stage has not completely transformed into the perpendicular tubes associated with the PMMA domains, thus signifying the beginning of the intermediate stage. In previous studies of PMMA/SAN films annealed for 0.5 h, AFM topographic measurements combined with PMMA etching was unable to directly observe PMMA tubes near the surface whereas Figure 3a shows tubes near the surface (red). A second new observation is apparent in the map of the sample annealed for 5 h which is well into the intermediate stage. Here, the morphology is dominated by PMMA domains (red) that span the film surface as previously determined by etching/topography mapping. However, BE-NanoTA imaging shows that small

SAN-rich domains appear trapped inside the larger PMMA domains (inset Figure S1d, Supporting Information). Neither the topography map taken before etching (Figure S1d, Supporting Information) or after etching revealed these trapped SAN domains. These two results point out the main disadvantage of the etching/topography approach, namely, the inability to directly image the PMMA phase and trapped SAN within the larger PMMA domains.

Figure 4 shows how the spatial resolution and sensitivity of BE-NanoTA compares with various techniques used in mechanical analysis including local thermal analysis (LTA) with Wollaston probe[5] and silicon heater;[6] local thermal analysis with silicon heater and band excitation detection, BE-NanoTA; and dynamic mechanical analysis, DMA.[4] Regions on spatial resolution/sensitivity map corresponding to different techniques are presented as a stack and arranged in an order of an area increase when techniques with larger spatial resolution−sensitivity range located at the bottom of the stack. The spatial resolution is limited by either the probe size in probe-based methods or the sample size in all other methods. Measurement of the displacement is a key component of all methods listed above; in Figure 4 we compared the sensitivities of all techniques in displacement measurements. Figure 4 also shows the spatial resolution and displacement sensitivity required for practical problems found in industrial applications, including analysis of pharmaceuticals, organic layers in OLEDS, lithography masks, mechanical properties of the surfaces (auto, optics etc.) (marked with blue/dark gray rectangle), and for basic scientific problems such as thermomechanical motion of single molecules (white/light ellipse). The spatial resolution and the sensitivity of Nano-TA are determined below. Recently, the spatial resolution for the local thermomechanical and T_g measurements is limited by the tip−surface contact radius, ~10 nm.[15] The vertical sensitivity level in static AFM (e.g., contact mode) is estimated as ~0.1 nm, which is mainly determined by the experimental noise limit for conventional photodetectors. For ac-detection methods based on amplitude or frequency detection, the vertical sensitivity as limited by the thermomechanical noise[32] is $\delta l_{tm} \approx (2k_B TB/k\omega_r)^{1/2}$, where k_B is the Boltzmann constant, T is temperature, B is the bandwidth, k is the cantilever spring constant, and ω_r is the cantilever resonant frequency. This yields the relationship between resolution and sensitivity as[25]

$$\frac{\delta l}{R_{contact}} \approx -(1+\nu)\alpha\delta T \quad (5)$$

where δl is the tip displacement due to thermal expansion of the material, $R_{contact}$ the radius of tip−surface contact, ν the Poisson ratio for surface material, and α the linear thermal expansion coefficient. The linear expansion coefficient (α) for SAN and PMMA are 6×10^{-4} K^{-1}[33] and $(1-2) \times 10^{-4}$ K^{-1},[34,35] whereas the Poisson's ratio for polymers is about 0.34. For the typical cantilever parameters $k \sim 1$ N/m, $\omega_r \sim 2\pi$ 300 kHz (contact resonance frequency), and $B \sim 1$ kHz (typical experimental bandwidth). Thus, for the temperature range 300−1000 K, the thermomechanical noise will be on the order of 3−10 pm.

Conclusion

To conclude, we demonstrate a nondestructive method, BE-NanoTA, that uses local thermal analysis of the polymer surface to measure the glass transition temperature with 50 nm lateral resolution. Moreover, BE-NanoTA provided insight into the early and intermediate stages of phase separation of SAN: PMMA films that was overlooked using an etching/topography mapping method. Because BE-NanoTA is nondestructive, phase evolution can be followed without chemical[17] or plasma[36] etching, which allows for in situ studies of polymer dynamics. Overlaying the capabilities of the mechanical analysis methods with industrial requirements (Figure 4) demonstrates that local thermal analysis with a silicon heater and band excitation detection, namely BE-NanoTA, significantly widens the applicability of local thermal analysis techniques. The theoretical spatial resolution of BE-NanoTA[25] approaches the length scale of the Kuhn segment length, and therefore a new understanding of the relationship between local segmental dynamics and mechanical properties may evolve from further studies. Thus, this paper demonstrates the potential of high-resolution mapping of thermal properties for investigating a range of technologically important areas ranging from quality control of coatings in drug delivery systems to characterizing new resists for semiconductor industry as well as fundamental issues such as single molecule thermomechanical analysis.

Acknowledgment. We thank L. T. Germinario for fruitful discussions of local thermal analysis and A. P. Baddorf for proofreading and restructuring the manuscript. A portion of this research at the Oak Ridge National Laboratory's Center for Nanophase Materials Sciences was sponsored by the Scientific User Facilities Division, Office of Basic Energy Sciences, U.S. Department of Energy. The BE-NanoTA technique is available as a part of user program at the CNMS. The work by R.J.C. and S.G. was supported by the Nano/Bio Interface Center at the University of Pennsylvania and the U.S. National Science Foundation (NSF) under Grant DMR08-32802 as well as the World Materials Network (NSF) DMR09-08449. Partial support was provided by the NSF Polymer program under Grant DMR09-07493.

Supporting Information Available: Topography of polymer films after 0, 0.5, 2, and 5 h of annealing. This material is available free of charge via the Internet at http://pubs.acs.org.

References and Notes

(1) Moss, S. J.; Ledwidth, A. *The Chemistry of the Semiconductor Industry*; Springer: New York, 1989.
(2) Uchegbu, I. F. *Polymers in Drug Delivery*; CRC: Boca Raton, FL, 2006.
(3) Peumans, P.; Uchida, S.; Forrest, S. R. *Nature* **2003**, *425* (6954), 158–162.
(4) Schlesing, W.; Buhk, M.; Osterhold, M. *Prog. Org. Coat.* **2004**, *49* (3), 197–208.
(5) Hammiche, A.; Price, D. M.; Dupas, E.; Mills, G.; Kulik, A.; Reading, M.; Weaver, J. M. R.; Pollock, H. M. *J. Microsc. (Oxford, U. K.)* **2000**, *199*, 180–190.
(6) Nelson, B. A.; King, W. P. *Rev. Sci. Instrum.* **2007**, *78* (2), 023702.
(7) Anasys Instruments.
(8) Zhu, S.; Liu, Y.; Rafailovich, M. H.; Sokolov, J.; Gersappe, D.; Winesett, D. A.; Ade, H. *Nature* **1999**, *400* (6739), 49–51.
(9) Priestley, R. D.; Ellison, C. J.; Broadbelt, L. J.; Torkelson, J. M. *Science* **2005**, *309* (5733), 456–459.
(10) Swallowe, G. M. *Mechanical Properties and Testing of Polymers: An A-Z Reference*; Kluwer: Dordrecht, 1999.
(11) Sperling, L. H. *Introduction to Physical Polymer Science*, 4th ed.; Wiley-Interscience: Hoboken, NJ, 2006.
(12) Rabe, U.; Amelio, S.; Kester, E.; Scherer, V.; Hirsekorn, S.; Arnold, W. *Ultrasonics* **2000**, *38* (1−8), 430–437.
(13) Oulevey, F.; Burnham, N. A.; Gremaud, G.; Kulik, A. J.; Pollock, H. M.; Hammiche, A.; Reading, M.; Song, M.; Hourston, D. J. *Polymer* **2000**, *41* (8), 3087–3092.
(14) Jesse, S.; Nikiforov, M. P.; Germinario, L. T.; Kalinin, S. V. *Appl. Phys. Lett.* **2008**, *93* (7), 073104.
(15) Nikiforov, M. P.; Jesse, S.; Morozovska, A.; Eliseev, E. A.; Germinario, L. T.; Kalinin, S. V. *Nanotechnology*, in press.
(16) Chung, H. J.; Composto, R. J. *Phys. Rev. Lett.* **2004**, *92* (18), 185704.
(17) Wang, H.; Composto, R. J. *Macromolecules* **2002**, *35* (7), 2799–2809.
(18) Wang, H.; Composto, R. J. *J. Chem. Phys.* **2000**, *113* (22), 10386–10397.
(19) Wang, H.; Composto, R. J. *Phys. Rev. E* **2000**, *61* (2), 1659–1663.
(20) Majumdar, A.; Carrejo, J. P.; Lai, J. *Appl. Phys. Lett.* **1993**, *62* (20), 2501–2503.
(21) Varesi, J.; Majumdar, A. *Appl. Phys. Lett.* **1998**, *72* (1), 37–39.
(22) Johnson, K. L. *Contact Mechanics*; Cambridge University Press: New York, 1987.

(23) Mark, J. E.; Ngai, K.; Graessley, W.; Mandelkern, L.; Samulski, E.; Koenig, J.; Wignall, G. *Physical Properties of Polymers*, 3rd ed.; Cambridge University Press: New York, 2004.
(24) Wei, P. J.; Shen, W. X.; Lin, J. F. *J. Non-Cryst. Solids* **2008**, *354* (33), 3911–3918.
(25) Nikiforov, M. P.; Jesse, S.; Morozovska, A. N.; Eliseev, E. A.; Germinario, L. T.; Kalinin, S. V. *Nanotechnology* **2009**, *20* (39), 395709.
(26) Moynihan, C. T.; Easteal, A. J.; Wilder, J.; Tucker, J. *J. Phys. Chem.* **1974**, *78* (26), 2673–2677.
(27) Alves, N. M.; Mano, J. F.; Ribelles, J. L. G.; Tejedor, J. A. G. *Polymer* **2004**, *45* (3), 1007–1017.
(28) Doulut, S.; Demont, P.; Lacabanne, C. *Macromolecules* **2000**, *33* (9), 3425–3430.
(29) Doulut, S.; Bacharan, C.; Demont, P.; Bernes, A.; Lacabanne, C. *J. Non-Cryst. Solids* **1998**, *235*, 645–651.
(30) Newby, B. M. Z.; Composto, R. J. *Macromolecules* **2000**, *33* (9), 3274–3282.
(31) Chung, H.; Ohno, K.; Fukuda, T.; Composto, R. J. *Macromolecules* **2007**, *40* (2), 384–388.
(32) Stroh, C.; Wang, H.; Bash, R.; Ashcroft, B.; Nelson, J.; Gruber, H.; Lohr, D.; Lindsay, S. M.; Hinterdorfer, P. *Proc. Natl. Acad. Sci. U.S.A.* **2004**, *101* (34), 12503−12507.
(33) Dlubek, G.; Pionteck, J.; Kilburn, D. *Macromol. Chem. Phys.* **2004**, *205* (4), 500–511.
(34) Brandrup, J.; Immergut, E. H. *Polymer Handbook* (*V-55*), 1st ed.; Wiley: New York, 1975.
(35) Zhai, J. F.; Qiu, L.; Zhou, J. Y.; Zhao, Y. X.; Shen, Y. Q.; Ling, Q. D.; Yang, M. J. *Adv. Mater. Opt. Electron.* **2000**, *10* (1), 3–7.
(36) Konrad, M.; Knoll, A.; Krausch, G.; Magerle, R. *Macromolecules* **2000**, *33* (15), 5518–5523.
(37) Jesse, S.; Kalinin, S. V.; Proksch, R.; Baddorf, A. P.; Rodriguez, B. J. *Nanotechnology* **2007**, *18* (43), 435503.
(38) Lee, J.; Beechem, T.; Wright, T. L.; Nelson, B. A.; Graham, S.; King, W. P. *J. Microelectromech. Syst.* **2006**, *15* (6), 1644–1655.